SUPPORTING INFORMATION

Silver Nanowire Exposure Results in Internalization and Toxicity to *Daphnia Magna*

Leona D. Scanlan[a], Robert B. Reed[b], Alexandre V. Loguinov[a], Philipp Antczak[c], Abderrahmane Tagmount[a], Shaul Aloni[d], Daniel Thomas Nowinski[a], Pauline Luong[a], Christine Tran[a], Nadeeka Karunaratne[a], Don Pham[a], Xin Xin Lin[a], Francesco Falciani[c], Chris P. Higgins[e], James F. Ranville[b], Chris D. Vulpe[a] Benjamin Gilbert[f]*

[a]University of California Berkeley, Department of Nutritional Sciences and Toxicology, 119 Morgan Hall, Berkeley, CA 94720

[b] Colorado School of Mines, Department of Chemistry and Geochemistry, 1500 Illinois St., Golden, CO

[c]University of Birmingham School of Biosciences, Edgbaston, Birmingham, B15 2TT, UK

[d]Molecular Foundry, Lawrence Berkeley National Laboratory, Materials Sciences Division, 1 Cyclotron Rd., MS 90-1116, Berkeley, CA, 94720

[e]Colorado School of Mines, Department of Civl and Environmental Engineering, Golden, CO 80401

[f]Earth Science Division, Lawrence Berkeley National Laboratory, Earth Sciences Division, 1 Cyclotron Rd., MS 74-316C, Berkeley, CA, 94720

* Address correspondence to vulpe@berkeley.edu

SUMMARY

Supporting Tables

Table S1 estimates nanorod and ionic silver contamination in AgNW stock.

Table S2 outlines *Daphnia* growth media components.

Table S3 shows Ag^{+}*(aq)* calculations in media.

Table S4 lists acute LC_{50} values of AgNWs in *Daphnia magna*.

Table S5 lists qPCR primer sequences.

Table S6 lists qPCR results.

Table S7, in a separate file, lists differentially expressed genes.

Table S8 lists affected transcripts for transporter proteins.

Table S9, a separate file, displays detailed results for the Blast2GO functional enrichment analysis.

Table S10 shows calculations for Ag^{+} contribution to AgNW toxicity.

Supporting Figures

Figure S1 is TEM imaging of PVP-AgNW and nanorod contamination.

Figure S2 shows aggregation of AgNW in solution.

Figure S3 shows AgNW settling rates.

Figure S4 is a TEM image showing morphological changes of the SiO_2-NW coating.

Figure S5 is TEM imaging of stock AgNWs and coatings.

Figure S6 is a Venn diagram showing numbers of gene expressed in common between different exposure conditions.

Figure S7 shows spICPMS data on nanowire length distribution.

Figure S8 shows an AgNP precipitate in Ag^{+}(aq)-exposed daphnid.

Figure S9 spICPMS data on nanoparticulate silver in hemolymph following Ag^{+}(aq) exposure.

Figure S10 is dark-field imaging of AgNWs.

Figure S11 is bright-field and dark-field imaging of the *D. magna* rostrum.

Figure S12 is bright-field and dark-field imaging of the *D. magna* anterior gut.

Figure S13 is bright-field imaging of the *D. magna* brood chamber.

Figure S14 shows dark-field imaging of AgNWs in the *D. magna* gut.

Figure S15 shows Ag^{+} retention in filters.

METHODS

Nanowire characterization. Transmission electron microscopy (TEM) and scanning transmission electron microscopy (STEM) were used to measure the morphology and dimensions of the nanowires and their surface coatings (Figures S1 & S5). The TEM (JEOL 2100F) was equipped with OXFORD INCA energy dispersive x-ray spectroscopy suite (EDS). STEM was equipped with Gatan's Digiscan II. TEM was also used to investigate the effects of aqueous medias on SiO_2 coating integrity. To do this, short SiO_2-NWs were immersed in exposure media for two hours. A droplet was placed on a lacey carbon grid, dried and imaged.

Elemental analysis. Imaging and elemental analysis of AgNW containing samples was performed with a scanning electron microscope (SEM) (Zeiss EVO) with an EDAX energy dispersive x-ray spectrometer (EDS). Individual AgNWs and aggregates were prepared on 5x5 mm silicon wafers (SPI Supplies) treated in a 5% HF solution or a 5% H_2SO_4 oxidizing solution (GODAX laboratories, Inc.) to generate, respectively, hydrophobic or hydrophilic surfaces. High-resolution imaging of NWs performed by collecting the secondary electron signal and limiting beam current to less than 100 pA. Sparse NWs in complex samples were located using the backscattered electron signal at approximately 1 nA, and their composition was established using EDAX from the Ag emission lines.

Aggregation and settling. Dynamic light scattering (DLS) (Precision Detectors) was used to measure the stability against aggregation of S-NW suspensions in *Daphnia* media and in pure water. The relative rates of AgNW settling were investigated by measuring the optical absorption spectroscopy (Ocean Optics) of unstirred 4-mL volumes of 12-mg/L suspensions

in closed 1-cm path-length quartz cuvettes. 1-mL aliquots were extracted for DLS analysis over a 48-hour period. All solutions were modestly stirred (1x5 mm stir bar at ~200 rpm) to limit NW settling. L-NW were too large for DLS analysis, so we collected L-NW and their aggregates from solution and imaged them using SEM on silicon wafers that had been treated with HF or oxidizing solution (described above) to generate hydrophilic or hydrophobic surfaces. At 12 mg/L Ag, collection time of 1-2 hours achieved a surface coverage of AgNW suitable for SEM imaging. All abiotic AgNW stability tests were performed using glass vials and quartz cuvettes.

Zeta potential. We measured the zeta potential of PVP- and silica-coated short nanowires dispersed in ultrapure water. Long nanowires were too large for analysis. Measurements were conducted with a Malvern Zetasizer 5000 in low volume disposable cuvettes. Particle size distributions were first measured using dynamic light scattering, using at least 20 measurements recorded to calculate a mean z average size. Provided the DLS measurement showed the sample to be free from dust or aggregates, dip-type electrodes were added for zeta potential measurements. At least 20 measurements were acquired until the data quality satisfied the software automatic assessment routine. We sought to measure the zeta potential of the nanowires in the EPA and COMBO media, but in all cases recorded zero potential, indicating the NW surfaces to be completely shielded from the applied electrostatic field in due to the non-zero ionic strength of these solutions.

Shaking *versus* still statistical significance. Raw acute data for long and short PVP-NW were compared with statistical software (GraphPad). For the L-PVP test, a paired, two-tail t-test was performed. Intermediate values used in calculations were a t-value of 0.1465, eight degrees of freedom and a standard error of difference of 1.516. A similar t-test was

performed on S-PVP data, with a t-value of 1.2623, 12 degrees of freedom and a standard error of difference of 0.488. Final p-values were 0.824 for S-PVP and 0.940 for L-PVP, indicating no statistical difference in daphnid lethality between still or shaken AgNW exposures.

Determination of differentially expressed gene candidates. Data were analyzed using a "Treatment *vs*. Control" design. Foreground intensities in each array were subtracted with local background. All negatives or flagged spots (using GenePix quality control flag system) were treated as missing values. All positive values were log (base-2)-transformed. Relative intensity ratios(treatment sample/control), or "M-values", were calculated for each gene (cDNA). Non-linear trends (if any) were corrected with loess global normalization.[1] Differential gene expression was determined with an algorithm based on α-outlier detection procedures.[2] Because microarray data are "noisy," a local variance estimator based on loess was used to take heteroscedasticity (if any) into consideration.[2] Each gene in a given "Treatment *vs*. Control" pair was characterized by two values: the normalized log-transformed ratio (fold change value) and the corresponding q-value (derived from p-values, which were adjusted for multiplicity of comparisons).[3] Fisher's method of meta-analysis was applied to combine p-values (this approach is scale-free and, as a result, does not require the use of between-array normalization). A multiple-slide method was used to detect candidate genes; the same technique was applied to all microarrays based on all possible combinations of a given treatment and the corresponding control biological replicates. This technique treated gene expression outcomes as Bernoulli trials (independent binary outcomes). Fisher's method-based p-values were adjusted with Bonferroni correction. A list of candidate genes was created for each treatment. All results were corrected for multiplicity of comparisons twice: 1) within a given "Experiment *vs*.

Control" pair, 2) across biological replicates. Candidate genes were annotated using Blast2Go.[4]

SUPPORTING TABLES

Sample	% passed through 0.45 µm	% passed through 0.02 µm = % ionic silver	Difference = % nanorod silver
S-PVP	2.2	0.6	1.6%
L-PVP	1.0	0.2	0.8%
S-SiO2	4.4	4.4	<0.1%
L-SiO2	0.5	0.4	<0.1%

Table S1. Estimate of the proportion of silver nanorods in AgNW suspensions.

200 uL of AgNW stock solution was added to 25 mL ultrapure water and stirred for about 10 minutes. Aliquots of each solution were passed through 0.45 µm or 0.02 µm diameter filters that retained just the AgNWs, or the AgNWs and nanorods, respectively. The filtered solutions were acidified with concentrated nitric acid and measured by ICP-MS for total silver.

COMBO			EPA	
Chemical	Concentration (mg/L)		Chemical	Concentration (mg/L)
$CaCl_2•2H_2O$	55		$NaHCO_3$	0.192
$MgSO_4•7H_2O$	55.5		$MgSO_4•7H_2O$	0.246
K_2HPO_4	4.36		$CaSO_4•2H_2O$	0.12
$NaNO_3$	42.5		KCl	0.008
$NaHCO_3$	50.5			
$Na_2SiO_3•9H_2O$	14.2			
H_3BO_3	12			

Table S2. Chemical compositions of the simulated freshwater media used in this study.

COMBO		EPA	
Species	Conc. in nM (µg/L)	Species	Conc. in nM (µg/L)
$AgCl^0$	5.1 (0.55)	Ag^+	7.8 (0.84)
Ag^+	3.8 (0.41)	$AgCl^0$	1.4 (0.15)
$AgCl_2^-$	0.3 (0.037)	$AgSO_4^-$	0.1 (0.014)
$AgSO_4^-$	0.013 (0.0014)	$AgCl_2^-$	0.013 (0.0014)

Table S3. Calculated concentrations of aqueous species containing silver for the EPA and COMBO simulated freshwater solutions.

Ranked in order of decreasing concentration. The pH was fixed at 8 and the total silver concentration was 1µg/L.

Media	Treatment	LC_{50} µg/L	95% confidence interval
COMBO	PVP-S	421.0	322.2 - 602.6
COMBO	PVP-L	233.9	210.1 - 257.2
COMBO	SiO2-S	155.0	140.5 - 169.2
COMBO	SiO2-L	522.0	404.0 - 638.3
COMBO	AgNO3	0.8	0.4 - 1.3
EPA	PVP-S	260.7	139.5 - 319.6
EPA	PVP-L	415.4	297.8 - 563.4
EPA	SiO2-S	3.6	1.7 - 5.8
EPA	SiO2-L	226.5	28.0 - 382.4
EPA	AgNO3	0.6	0.28 - 1.2

Table S4. Acute 24-hour LC_{50} values for AgNWs on *Daphnia magna* determined by probit analyses.

Each LC_{50} is representative of at least 12 replicates of six AgNW exposure concentrations containing five daphnids each.

Nickname	Reason	Protein	Changes	Direction	Sequence
7657	all affected	unknown	all down	Forward Reverse	GGGGTGGCCATCGCTGTTAGTC TCCATCGCGGCATCGTCCACT
7499	fold change	unknown	LP-, SP-	Forward Reverse	AACCTCTGCCAACCAGCCGTT CGCCGACGGCCTCCATGATT
2267	q-value	carbonic anhydrase	LP-	Forward Reverse	AGCAGCTCGAATCTTTCCGCGA TGCTCAACCGACAACGGTGGG
4057	fold change	conidiospore surface protein	LP+. SS-	Forward Reverse	CGGTGGCGATTACGTTCCTTCACC GCGCGAGGGTAATAGGGGGC
1395	mode of tox	ribosomal	LS+, SS+	Forward Reverse	TACGAGCTTCGGACGAGCCCT TCCCCGTGCAGCAAAGACAAGG
18S	mode of tox	ribosonal	Ag+?	Forward Reverse	CGC TCT GAA TCA AGG GTG TT AAC CCC GAA GAG GAA GAA AA
GAPDH	house	GAPDH	n/a	Forward Reverse	GGGGACAGACGTTTCCTGTA AAGGGGTCATTGACAGCAAC
actin	house	actin	n/a	Forward Reverse	GGTATGTGCAAGGCTGGATT GGTGTGGTGCCAGATCTTTT

Table S5. List of genes and corresponding primers used in qPCR verification of microarray data.

Sample	GAPDH	4057/ fold	dCt	2^-dCt	Average	P-Value
con	23.720	33.740	10.020	0.001	0.001	
con	24.380	33.750	9.370	0.002		
con	24.620	33.720	9.100	0.002	Fold Change	
SS	22.740	32.560	9.820	0.001	0.772	0.097
SS	22.800	33.290	10.490	0.001	0.485	
SS	21.370	32.290	10.920	0.001	0.360	
Sample	GAPDH	7657/ all down	dCt	2^-dCt	Average	P-Value
con	23.720	25.010	1.290	0.409	0.378	
con	24.620	26.150	1.530	0.346	Fold Change	
Ag	23.270	24.700	1.430	0.371	0.983	0.588
Ag	22.780	24.340	1.560	0.339	0.898	
SS	22.740	24.700	1.960	0.257	0.681	0.072
SS	22.800	24.860	2.060	0.240	0.635	
SS	21.370	24.560	3.190	0.110	0.290	
LS	22.760	25.160	2.400	0.189	0.502	0.273
LS	22.720	24.310	1.590	0.332	0.880	
SP	22.050	28.420	6.370	0.012	0.032	0.002
SP	22.930	26.790	3.860	0.069	0.182	
SP	23.260	27.590	4.330	0.050	0.132	
Sample	actin	1395/ brix	dCt	2^-dCt	Average	P-Value
con	21.980	26.790	4.810	0.036	0.043	
con	22.540	26.830	4.290	0.051	Fold Change	
SS	21.110	25.120	4.010	0.062	1.431	0.580
SS	19.850	24.440	4.590	0.042	0.957	
LS	20.810	26.460	5.650	0.020	0.459	0.026
LS	20.420	26.280	5.860	0.017	0.397	

LS	20.890	26.540	5.650	0.020	0.459	
Sample	actin	18S ribosome	dCt	2^-dCt	Average	P-Value
con	21.980	12.730	-9.250	608.874	499.798	
con	22.540	13.930	-8.610	390.722	Fold Change	
Ag	22.060	12.070	-9.990	1016.927	2.035	0.442
Ag	21.980	12.990	-8.990	508.463	1.017	
Sample	actin	7499/ fold	dCt	2^-dCt	Average	P-Value
con	21.980	26.400	4.420	0.047	0.060	
con	22.540	26.300	3.760	0.074	Fold Change	
SP	19.430	27.690	8.260	0.003	0.054	0.068
SP	20.530	26.810	6.280	0.013	0.214	
LP	20.200	26.930	6.730	0.009	0.156	0.016
LP	20.920	27.440	6.520	0.011	0.181	
LP	21.700	28.430	6.730	0.009	0.156	
Sample	actin	2267/q-value	dCt	2^-dCt	Average	
con	21.980	23.920	1.940	0.261	0.398	P-Value
con	22.540	23.440	0.900	0.536	Fold Change	
LP	20.200	23.420	3.220	0.107	0.269	0.081
LP	20.920	23.640	2.720	0.152	0.381	
LP	21.700	24.690	2.990	0.126	0.316	
Sample	actin	4057/ fold	dct	2^-dct	Average	P-Value
con	24.320	35.790	11.470	0.000	0.001	
con	25.600	35.870	10.270	0.001		
con	25.160	35.580	10.420	0.001	Fold Change	
LP	24.380	23.430	-0.950	1.932	3062.721	0.161
LP	24.970	26.660	1.690	0.310	491.347	
Sample	actin	1395/ brix	dCt	2^-dCt	Average	P-Value

con	21.070	26.000	4.930	0.033	0.052	
con	21.950	25.770	3.820	0.071	Fold Change	
SS	20.490	24.230	3.740	0.075	1.445	0.724
SS	20.370	24.760	4.390	0.048	0.921	
LS	20.090	25.550	5.460	0.023	0.439	0.129
LS	20.140	25.510	5.370	0.024	0.467	
LS	20.180	25.880	5.700	0.019	0.371	

Table S6. Results from RT-q-PCR analysis.

Green highlights indicate agreement with microarray data, red indicates disagreement and blue indicates variation in results. All primers tested agreed with array data except for primer 1395, a protein associated with ribosomal biogenesis.

Table S7. The complete list of differentially expressed genes and BLAST analysis.

Located in a separate file (Scanlan Supplement S7) due to size of file. S7 contains fold-change and q-value information.

GeneID	Protein Function	L-PVP	L-SiO2	S-PVP	S-SiO2	Ag+
DM02485P1	Solute Carrier	-0.6				
DM05687P2	ABC related					-3.2
DM01730P3	Calcium transporting ATPase					-1.9
DM06992P4	Iron(III) dicitrate permease protein fecC		1.1			
DM06914P2	Fe Transport			-2.4	-1.4	
DM04501P3	sodium-dependent phosphate transporter			-0.2		
DM02022P2	Na/K-transporting ATPase subunit alpha			-1.1		
DM01589P2	Na/K-transporting ATPase subunit alpha				-0.7	
DM03514P2	sodium/solute symporter			-0.5		

Table S8. Probes identified by BLAST as transporter proteins that were differentially expressed in response to AgNW exposure.

Red: sodium transporters; blue: other transporters.

Table S9. Detailed results for the Blast2Go functional enrichment analysis.

Data are found in a separate excel file, Scanlan Supplement S9.

	Abiotic Ag^+ release data						
Exposure	Ag added as NW (ug/L)	Ag^+ released (ug/L)	Fraction released	NW LD_{50} (ug/L)	Expected Ag^+ release at LD_{50}	Ag^+ LD_{50} (ug/L)	$[Ag^+]$ / Ag^+ LD_{50}
AgNW-S-SiO2 COMBO	12,000	8.9	0.00074	155	0.115	0.8	0.14
AgNW-S-SiO2 EPA	12,000	2.7	0.00022	3.6	0.00081	0.6	0.0014
AgNW-S-PVP EPA	12,000	1.6	0.00013	260.7	0.0347	0.6	0.058
AgNW-L-SiO2 EPA	12,000	0.3	0.000025	226.5	0.0056	0.6	0.0094

Table S10. Estimation of the contribution of Ag^+ to AgNW toxicity.

For each sample, the amount of Ag^+ released in abiotic trials at a concentration of 12 mg/L Ag (*c.f.* Figure 2) is scaled proportionally to the LD_{50} concentrations of AgNWs for the same sample and media. The last column reports the ratio between the LD_{50} for dissolved silver and the concentration of dissolved predicted released silver for each AgNW sample. Because all values are less than unity, typically much less than unity, Ag^+ release in solution cannot be the major cause of toxicity.

SUPPORTING FIGURES

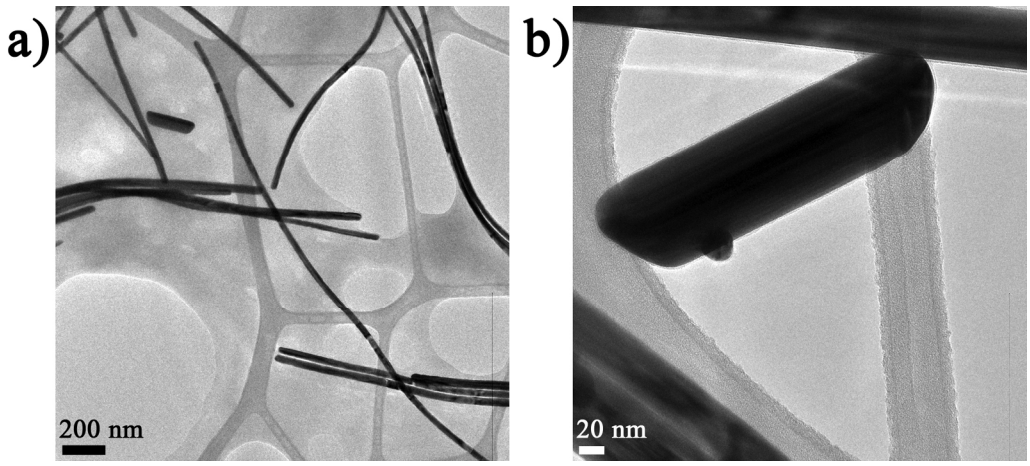

Figure S1. Transmission electron microscope images of PVP-coated silver nanorod impurities observed in the short (2 μm long) AgNW sample.

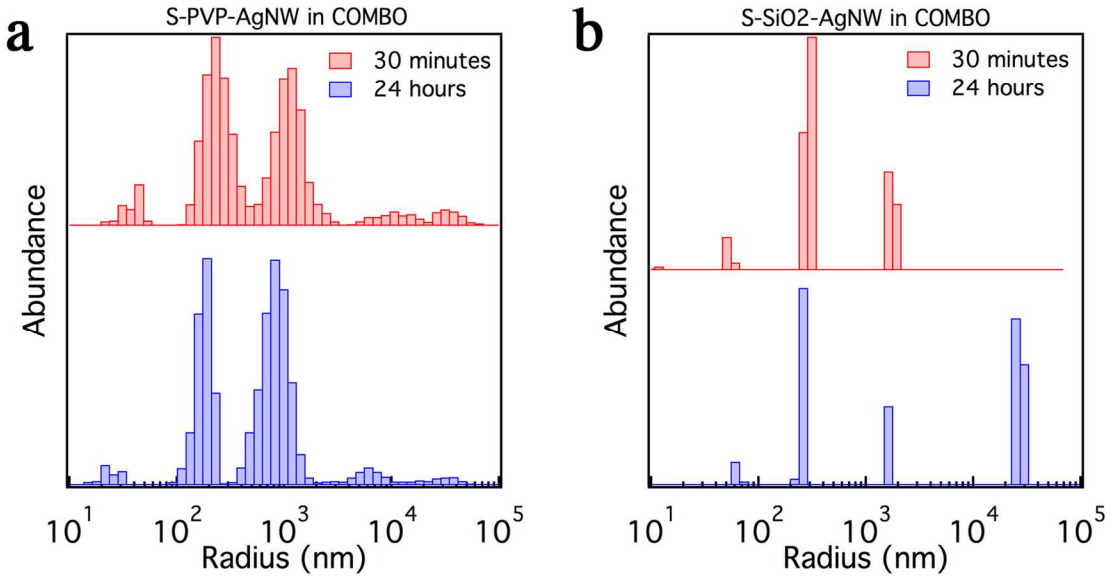

Figure S2. Dynamic Light Scattering (DLS) observation of the stability of (a) PVP-NW and (b) SiO_2-NW in COMBO media. Initially, both samples contained a proportion of individual nanowires and small aggregates. After 24 hours, no change in aggregation state of S-PVP-NW was observed. By contrast, micron-scale aggregates of S-SiO_2-NW appeared after this time. Aggregation and settling for S-SiO_2-NW in EPA was significantly more pronounced, leading to poor quality DLS data (not shown).

Note: the algorithm used to transform DLS correlation functions to hydrodynamic radii assumed spherical particle morphology, and hence the horizontal axis is not accurate.

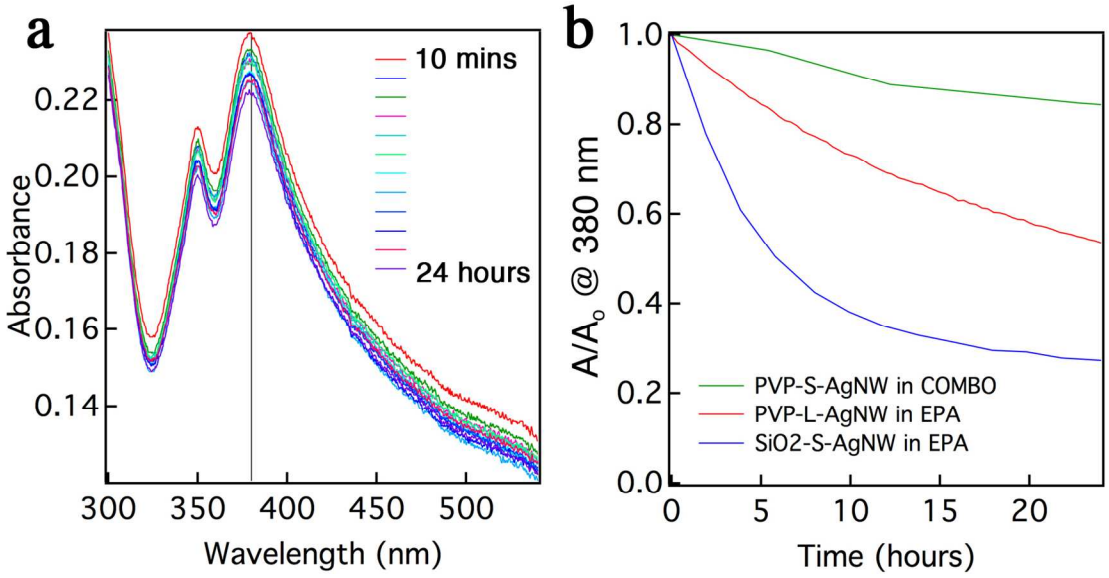

Figure S3. UV-vis determination of relative settling rates of AgNWs in *Daphnia* growth media. (a) Series of optical absorption spectra acquired from unstirred suspension of L-PVP-NW in COMBO media. The AgNW exhibited two characteristic surface plasmon resonance peaks. (b) Time dependent drop in absorbance (a) due to AgNW settling, monitored at 380 nm in a 1-cm pathlength cuvette with the beampath 1.5 cm beneath the solution meniscus.

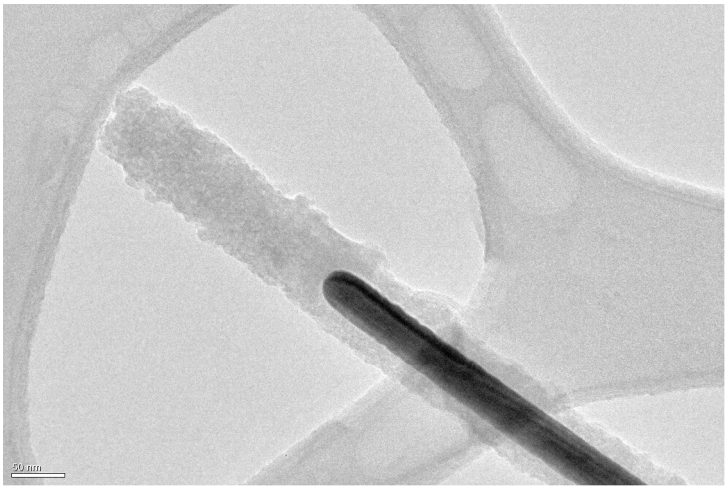

Figure S4. Transmission electron microscope image of a SiO_2-coated AgNW shows morphological changes in the silica coating.

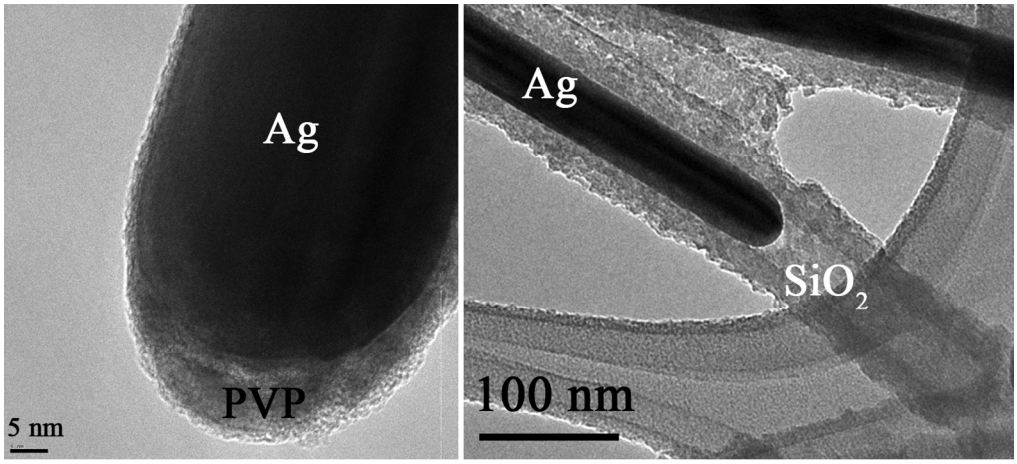

Figure S5. Transmission electron microscopy of (left) poly(vinylpyrrolidone)-coated (PVP) and (right) amorphous aluminum-doped silica-coated (SiO_2) AgNWs taken from the stock solutions. All SiO_2-NW exhibited enclosed voids at the tip, caused by preferential etching of silver during the removal of PVP and precipitation of the inorganic coating. The SiO_2 coatings were stable in the anaerobic stock solution.

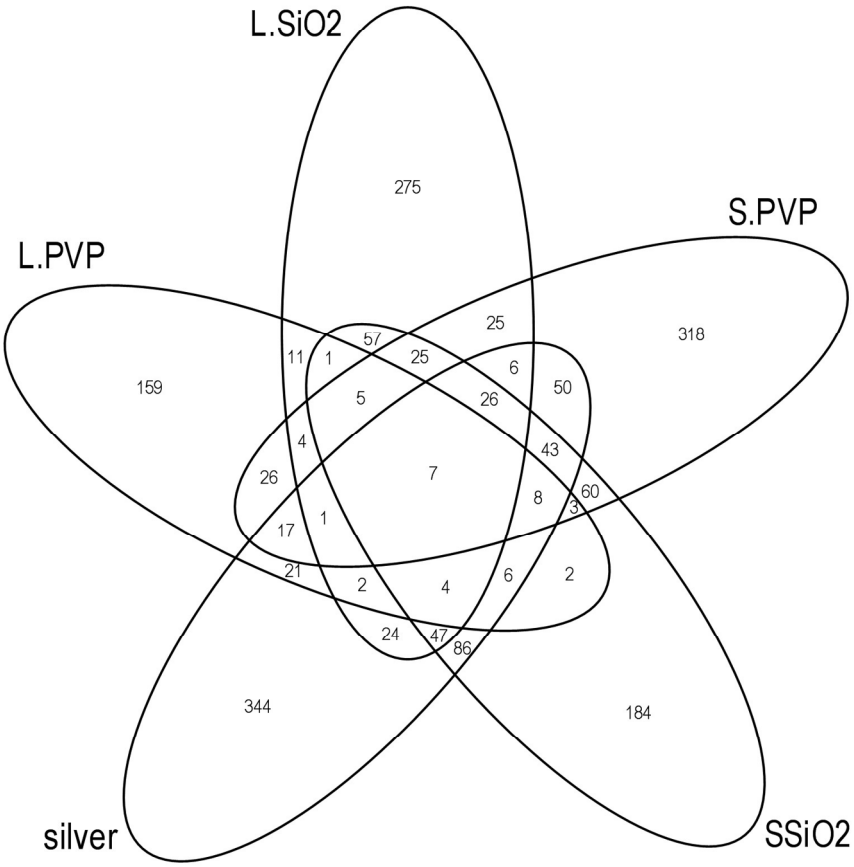

Figures S6. Venn diagram of differentially expressed genes in each as compared to the media-only control. Gene commonly expressed in only the AgNW exposures may be useful biomarkers of exposure.

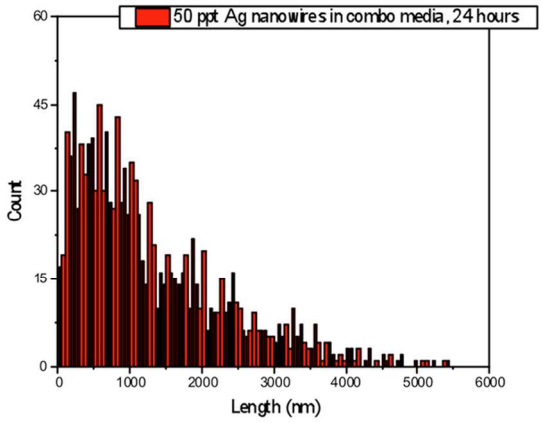

Figure S7. spICPMS data on silver nanowire length distribution. ~2-µm-long silica-coated AgNWs in COMBO media (S-SiO_2-NW).

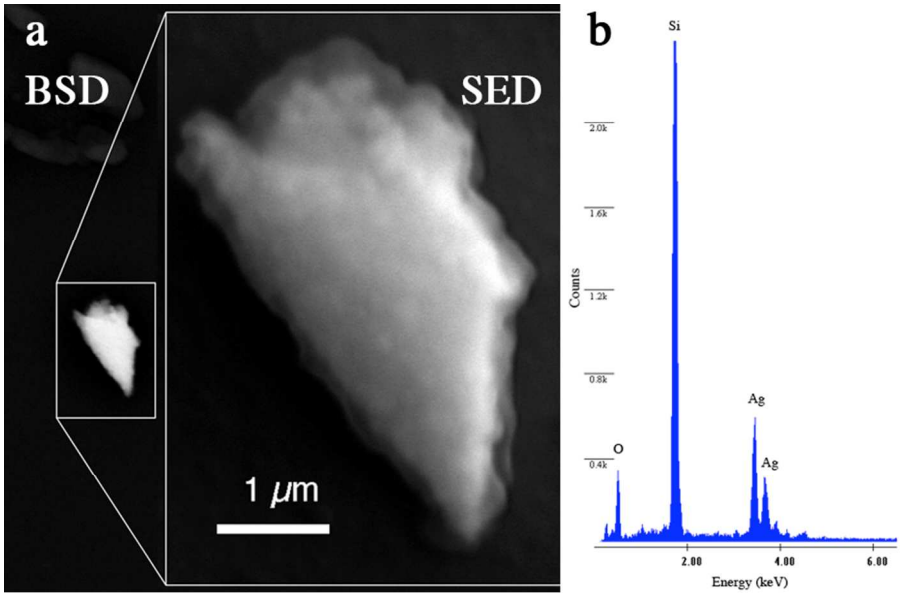

Figure S8. Scanning electron microscope analysis of a silver-rich precipitate located in the dried hemolymph of a daphnid exposed to ~2-µm-long silica-coated AgNWs at the LC_{50} concentration. **(a)** Precipitate imaged using the back-scattering detector (BSD) and secondary electron detector (SED). **(b)** X-ray fluorescence signal from the precipitate.

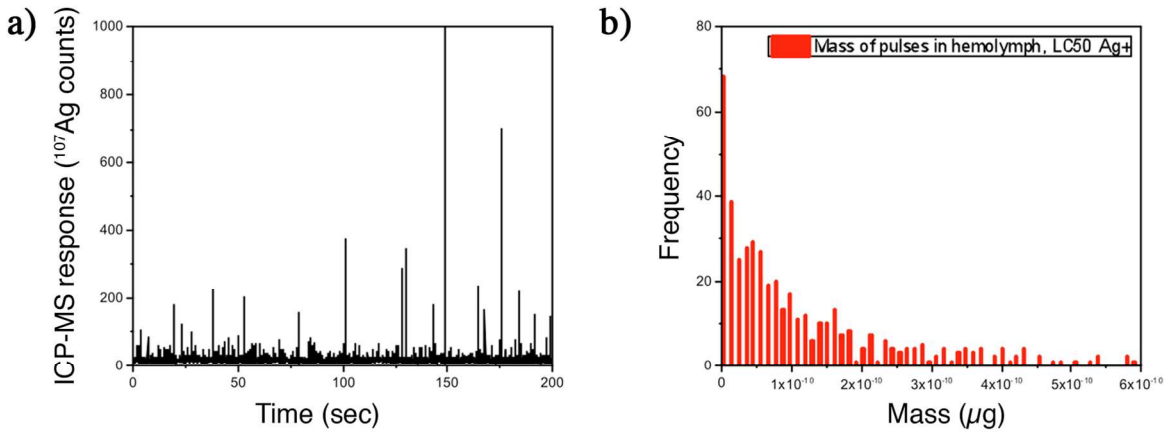

Figure S9. Nanoparticulate silver in hemolymph following Ag^+(*aq*) exposure. a) Raw data from spICPMS analysis of diluted hemolymph from daphnids exposed to the LC_{50} for silver nitrate. **b)** Corresponding distribution of particulate masses (assuming pure Ag).

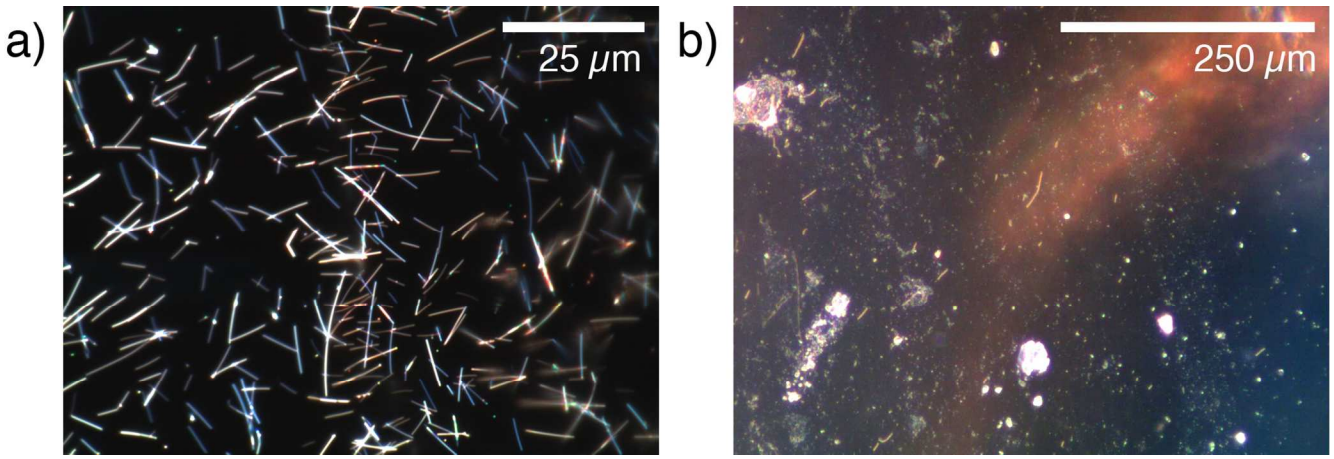

Figure S10. **PVP-coated AgNWs were detectable using optical light microscopy in dark-field mode. a)** Dark-field micrograph of PVP-coated AgNW in COMBO medium. 100x objective. **b)** Dark-field micrograph of AgNW in COMBO following the addition of 4% paraformaldehyde and a 3-hour fixation period. The fixative caused all NWs to lose their luster. Following fixation, only AgNWs that adhered to the glass slide were detectable; no daphnid-associated AgNW could be identified.

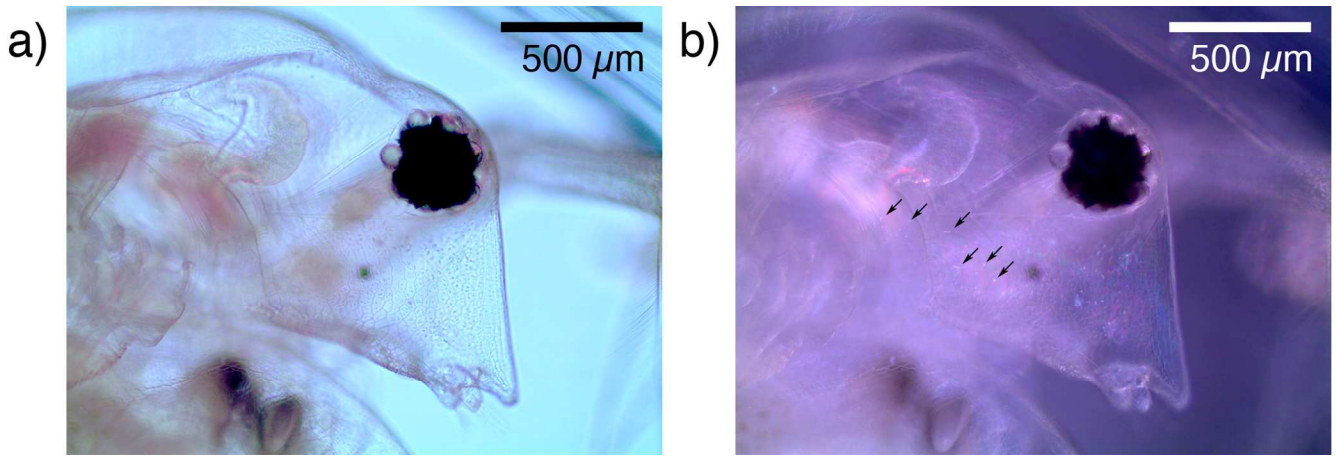

Figure S11. **AgNWs in the *D. magna* rostrum.** Daphnid head imaged in **a)** bright-field and **b)** dark-field mode. Arrows in **b)** indicate individual mobile AgNW.

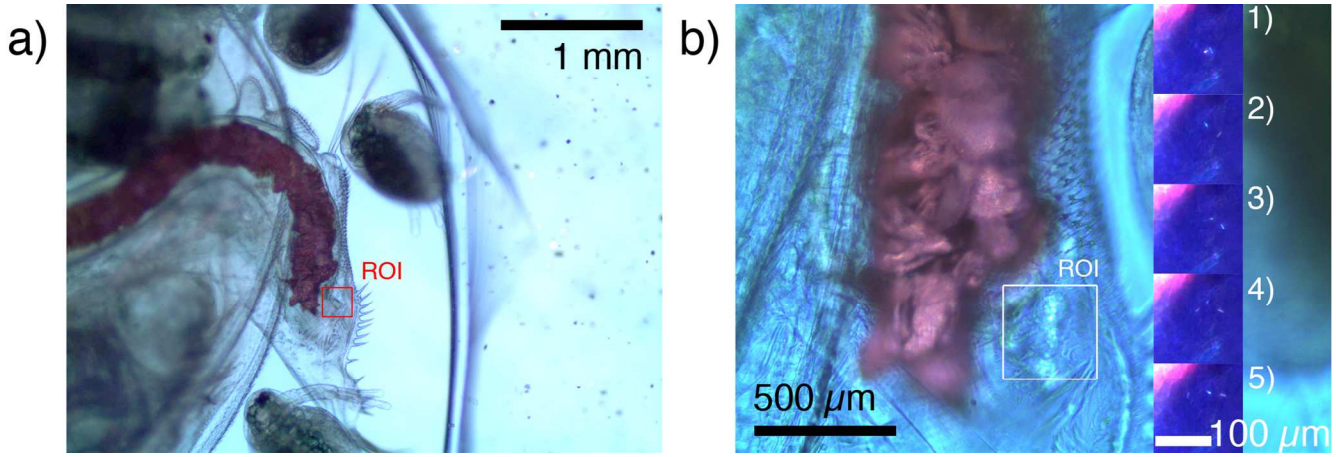

Figure S12. **AgNW in the gut anterior.** Dark-field imaging of the anterior region of the gut of AgNW-exposed daphnids revealed freely-diffusing AgNWs. **a)** Bright-field image at low-magnification, showing region-of-interest (ROI; red box). **b)** Higher-magnification dark-field images. The sequence of images 1-5 captured over approximately 3 minutes show a number of internal AgNW to be moving.

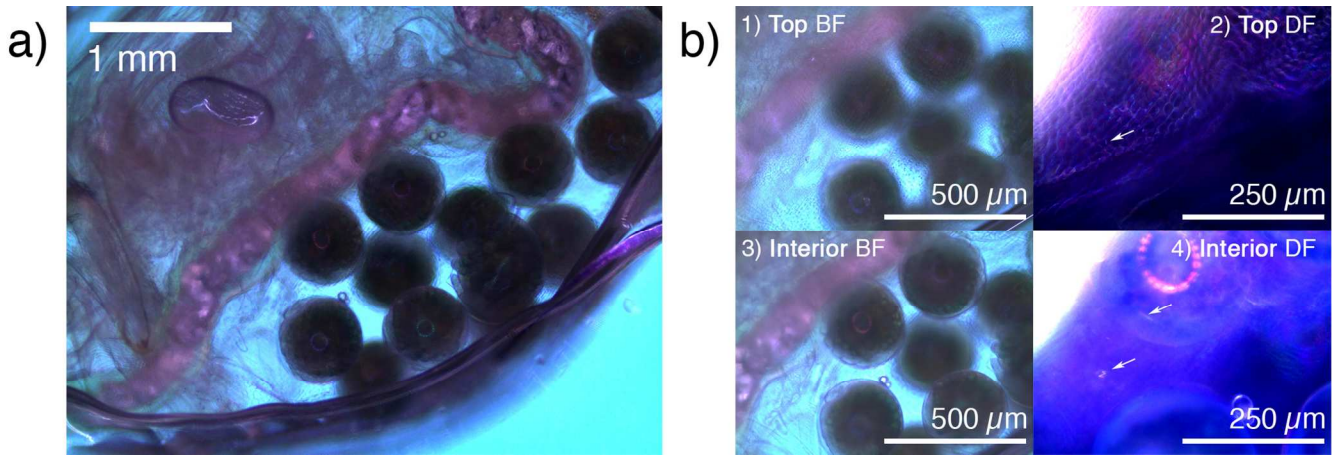

Figure S13. **AgNW in the brood chamber. a)** Bright-field image at low-magnification showing eggs in the brood hatch behind the gut. **b)** Stationary AgNWs adhering to the daphnid exterior (top image pair), and moving AgNWs inside the brood hatch (bottom image pair) could be distinguished by adjusting the microscope focus.

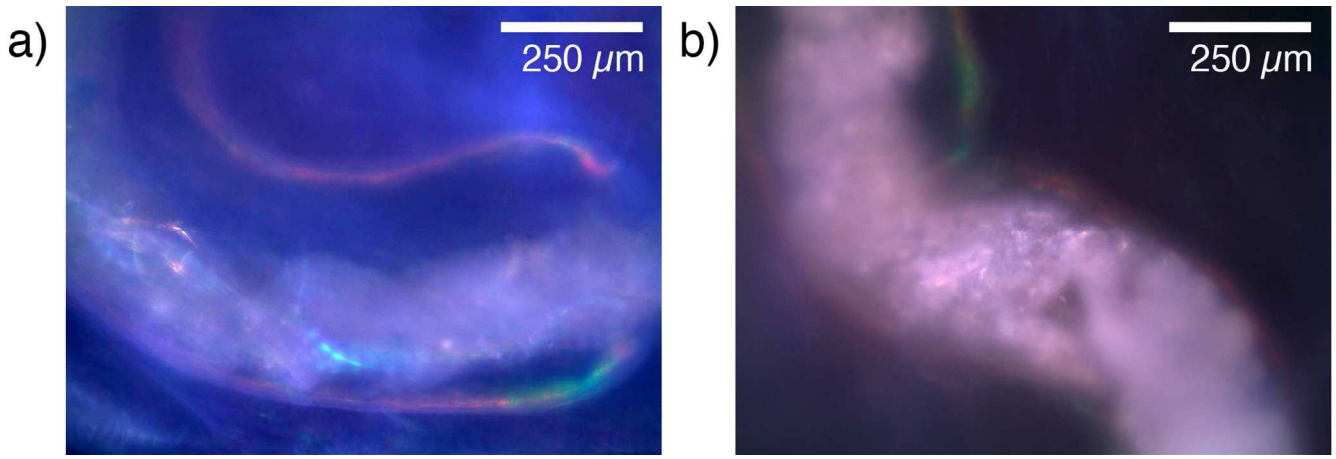

Figure S14. **Dark-field imaging of daphnid gut.** Dark-field imaging of the gut of **a)** control and **b)** AgNW-exposed daphnids. Few putative AgNWs could be imaged in the gut of the exposed organisms. However, the entire gut contents of the exposed individuals gave much brighter signal in the dark-field mode than the control. The gut contents appeared to be consistent with aggregated or transformed AgNWs closely associated with food, in which individual AgNWs could not be resolved with the resolution of the optical microscope.

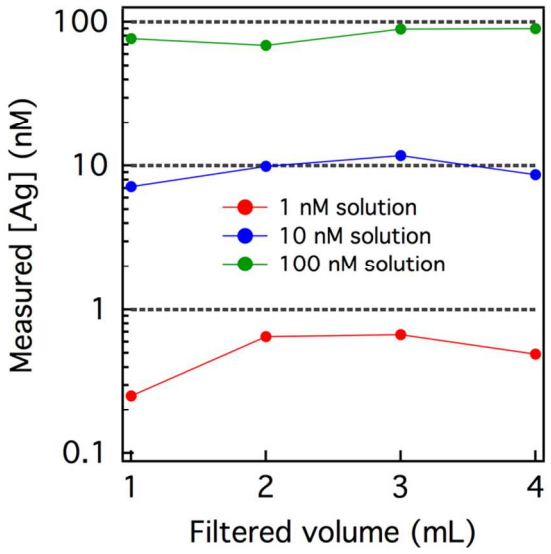

Figure S15. Tests of $Ag^{+}(aq)$ retention in the 0.2-µm filters used to remove AgNWs from suspension prior to elemental analysis of dissolved silver. We passed four 1-mL aliquots of 1, 10 or 100 nM standard silver nitrate solutions through a fresh filter and analyzed each aliquot for total silver.

REFERENCES

1. Yang, Y. H.; Dudoit, S.; Luu, P.; Lin, D. M.; Peng, V.; Ngai, J.; Speed, T. P., Normalization For cDNA Microarray Data: A Robust Composite Method Addressing Single and Multiple Slide Systematic Variation. *Nucleic Acids Res*. 2002, 30, e15-24.

2. Loguinov, A. V.; Mian, I. S.; Vulpe, C. D., Exploratory Differential Gene Expression Analysis in Microarray Experiments With No or Limited Replication. *Genome Biol*. 2004, 5, R18-33.

3. Storey, J. D.; Tibshirani, R., Statistical Significance for Genomewide Studies. *Proc. Natl. Acad. Sci. U. S. A.* 2003, 100, 9440-9445.

4. Conesa, A.; Gotz, S.; Garcia-Gomez, J. M.; Terol, J.; Talon, M.; Robles, M., Blast2GO: A Universal Tool for Annotation, Visualization and Analysis in Functional Genomics Research. *Bioinformatics* 2005, 21, 3674-3676.